Low-lying spectroscopy of a few even-even silicon isotopes investigated with the multiparticle-multihole Gogny energy density functional

N. Pillet,[1] V. G. Zelevinsky,[2] M. Dupuis,[1] J.-F. Berger,[1] and J. M. Daugas[1]

[1]*CEA, DAM, DIF, F-91297 Arpajon, France*

[2]*Department of Physics and Astronomy and National Superconducting Cyclotron Laboratory, Michigan State University, East Lansing, Michigan 48824, USA*

(Received 13 October 2011; revised manuscript received 29 December 2011; published 16 April 2012)

A multiconfiguration microscopic method has been applied with the Gogny effective interaction to the calculation of low-lying positive-parity states in even-even $^{26-32}$Si isotopes. The aim of the study is to compare the results of this approach with those of a standard method of generator coordinate method (GCM) type and to get insight into the predictive power of multiconfiguration methods employed with effective nucleon-nucleon force tailored to mean-field calculations. It is found that the multiconfiguration approach leads to an excellent description of the low-lying spectroscopy of ^{26}Si, ^{28}Si, and ^{32}Si, but gives a systematic energy shift in ^{30}Si. A careful analysis of this phenomenon shows that this discrepancy originates from too large proton-neutron matrix elements supplied by the Gogny interaction at the level of the approximate resolution of the multiparticle-multihole configuration mixing method done in the present study. These proton-neutron matrix elements enter in the definition of both single-particle orbital energies and coupling matrix elements. Finally, a statistical analysis of highly excited configurations in ^{28}Si is performed, revealing exponential convergence in agreement with previous work in the context of the shell model approach. This latter result provides strong arguments toward an implicit treatment of highly excited configurations.

DOI: 10.1103/PhysRevC.85.044315 PACS number(s): 21.60.Jz, 21.30.Fe, 27.60.+j

I. INTRODUCTION

Mean-field approaches provide a reliable foundation for an approximate solution of the nuclear many-body problem. Nowadays, a lot of effort is applied to move beyond the mean-field approximation and account for missing correlations. Special attention is paid to the restoration of symmetries broken in mean-field approaches [1–9], for example using projection techniques. An alternative way is to develop a theory in which the trial wave functions preserve certain symmetries. In particular, this can be achieved by multiconfiguration methods widely used in various applications, including atomic, molecular, and condensed matter physics. When the interaction is known, this kind of approach provides a very accurate description of a system. In a previous work [10], we proposed in the nuclear physics context a variational approach based on multiparticle-multihole (mp-mh) proton and neutron configuration mixings that uses the two-body finite-range density-dependent Gogny interaction in a fully microscopic way. As a first step, the method was applied in a particular case: pairing correlations (proton-proton and neutron-neutron) were investigated for the ground states of several even-even tin isotopes. A pioneering work using the Skyrme SIII interaction for the mean-field part and a schematic contact interaction for the residual part has been directed to the description of K isomers in the ^{178}Hf mass region [11].

The main objective of the present study is twofold: first, to test the ability of mp-mh multiconfiguration approach to describe low-lying nuclear states and second, to discuss the statistical features of highly excited configurations in nuclei. With this aim in view, a few silicon isotopes have been chosen and their excited states calculated with the mp-mh approach. Concerning highly excited configurations, the leading idea is to investigate whether exponential convergence behavior, revealed in the standard shell model (SM) approach [12–16], also emerges from variational (mp-mh) configuration mixing methods [10] in which single particle excitations are not restricted to a single major shell.

As practical calculations inevitably require some truncation of the orbital space and order of excitation, the mp-mh method proposes a promising scheme that allows one to predict the energies of low-lying states in a very accurate way. The possible use of statistical properties of highly excited states, which display generic signatures of quantum chaos close to random matrix theory, drastically reduces the sizes of the explicit diagonalizations. In the literature, one finds other approaches proposing different algorithms as, for example, the density matrix renormalization group [17–21] or Monte Carlo techniques [22], selecting the most relevant configurations for the description of many-body states.

The paper is organized as follows. The main characteristics of the mp-mh multiconfiguration approach applied in this study are presented in Sec. II. In Sec. III, the results obtained with the mp-mh approach for low-lying states in $^{26-32}$Si are presented and compared with those derived from a five-dimensional approximate generator coordinate method (GCM) approach (Secs. III A and III B). Differences between theoretical and experimental results are discussed. In particular, the systematic energy shift found in ^{30}Si is analyzed in terms of proton-neutron matrix elements. Section III C highlights the crucial role played by the residual interaction between protons and neutrons. Section IV is devoted to the analysis of the statistical properties of highly excited configurations, taking ^{28}Si as an example. Conclusions and perspectives are given in Sec. V.

II. MULTIPARTICLE-MULTIHOLE CONFIGURATION MIXING APPROACH

In this part, we discuss a few characteristics of the mp-mh configuration mixing approach. A general derivation of the corresponding formalism in nuclear physics, with two-body density-dependent interactions, has been introduced in Ref. [10]. It is worth to recall here the basics of the method not only to fix notations but also to provide an alternative formulation of equations in terms of a "core + valence space" description.

In the mp-mh configuration mixing method, the effective Hamiltonian is defined as a functional

$$\hat{H}(\rho) = \hat{K} + \hat{V}(\rho) \tag{1}$$

of the single-particle density matrix ρ. In Eq. (1), the Hamiltonian contains a kinetic term $\hat{K}$ (which includes the one-body center-of-mass corrections) and a two-body density-dependent potential term $\hat{V}(\rho)$ (which includes the Coulomb potential for protons as well as the two-body center-of-mass corrections). In our study, the D1S Gogny interaction [23] is adopted.

The trial wave functions $|\Psi\rangle$ that describe nuclear stationary states are expressed as linear combinations

$$|\Psi\rangle = \sum_{\alpha_\pi \alpha_\nu} A_{\alpha_\pi \alpha_\nu} \left|\phi_{\alpha_\pi} \phi_{\alpha_\nu}\right\rangle \tag{2}$$

of direct products

$$\left|\phi_{\alpha_\pi} \phi_{\alpha_\nu}\right\rangle = \left|\phi_{\alpha_\pi}\right\rangle \otimes \left|\phi_{\alpha_\nu}\right\rangle \tag{3}$$

of proton and neutron Slater determinants, $|\phi_{\alpha_\pi}\rangle$ and $|\phi_{\alpha_\nu}\rangle$ respectively, containing *a priori* any multiple p-h excitations that respect conserved quantum numbers.

Equation (2) contains two sets of unknown parameters, the mixing coefficients $A_{\alpha_\pi \alpha_\nu}$ and the single-particle orbitals. Both are determined by applying a variational principle to a functional $\mathcal{F}(\rho)$ related to the total energy of the system,

$$\mathcal{F}(\rho) = \langle\Psi|\hat{H}(\rho)|\Psi\rangle - \lambda\langle\Psi|\Psi\rangle - \sum_i \lambda_i Q_i, \tag{4}$$

where λ and λ_i are Lagrange multipliers and Q_i possible additional constraints that we will leave out in the following. One assumes that the one-body density ρ entering the effective Hamiltonian $\hat{H}(\rho)$ is the correlated one: $\rho = \langle\Psi|\hat{\rho}|\Psi\rangle$.

The minimization of $\mathcal{F}(\rho)$ with respect to the $A_{\alpha_\pi \alpha_\nu}$ leads to a nonlinear secular equation that is equivalent to a diagonalization problem in the multiconfigurational space of a Hamiltonian matrix $\mathcal{H}$,

$$\sum_{\alpha'_\pi \alpha'_\nu} \mathcal{H}_{\alpha_\pi \alpha_\nu, \alpha'_\pi \alpha'_\nu} A_{\alpha'_\pi \alpha'_\nu} = \lambda A_{\alpha_\pi \alpha_\nu}. \tag{5}$$

In Eq. (5), the matrix $\mathcal{H}$ contains contributions of the Hamiltonian $\hat{H}(\rho)$ and of rearrangement terms that come from the density dependence of the interaction,

$$\mathcal{H}_{\alpha_\pi \alpha_\nu, \alpha'_\pi \alpha'_\nu} = \left\langle \phi_{\alpha_\pi} \phi_{\alpha_\nu} \middle| \hat{H}(\rho) + \sum_{mn\tau} \mathcal{R}^\tau_{mn} a^+_{\tau m} a_{\tau n} \middle| \phi_{\alpha'_\pi} \phi_{\alpha'_\nu} \right\rangle, \tag{6}$$

where the summation over τ specifies the proton and neutron contributions to the generalized rearrangement terms with coefficients $\mathcal{R}^\tau_{mn}$. It is the presence of the rearrangement terms that transforms Eq. (5) into a nonlinear eigenvalue problem. As can be seen from Eq. (A5), the rearrangement terms contain contributions associated with the one-body density ρ and the two-body correlation matrix σ defined by

$$\sigma_{ij,kl} = \langle\Psi|a^+_i a^+_k a_l a_j|\Psi\rangle - \rho_{ji}\rho_{lk} + \rho_{jk}\rho_{li}. \tag{7}$$

In the Appendix, we express Eqs. (5) and (6) in a "core + valence space" scheme, a form which is explicitly used in the present study.

The minimization of $\mathcal{F}(\rho)$ with respect to the single-particle orbitals leads to inhomogeneous Hartree-Fock (HF) equations which depend on the amount of correlations contained in $|\Psi\rangle$ [10],

$$[h(\rho,\sigma), \rho] = G(\sigma), \tag{8}$$

where

$$G_{kl}(\sigma) = \frac{1}{2}\sum_{imn}\langle im|V(\rho)|kn\rangle\sigma_{il,mn} - \frac{1}{2}\sum_{imn}\langle ml|V(\rho)|\widetilde{ni}\rangle\sigma_{ki,mn}. \tag{9}$$

In Eq. (8), $h(\rho,\sigma)$ is the one-body mean-field Hamiltonian built with the one-body density ρ and the two-body correlation matrix σ:

$$h_{ij}(\rho,\sigma) = \langle i|K|j\rangle + \Gamma_{ij}(\rho) + \partial\Gamma_{ij}(\rho) + \partial\Gamma_{ij}(\sigma). \tag{10}$$

Explicit expressions for the fields $\Gamma_{ij}(\rho)$, $\partial\Gamma_{ij}(\rho)$, and $\partial\Gamma_{ij}(\sigma)$ are given in Ref. [10]. The basis that diagonalizes $h(\rho,\sigma)$ provides proton and neutron single-particle orbitals with energies ϵ^τ_i. The diagonal part of Eq. (6), that is the one obtained by taking $\alpha \equiv \alpha'$, can be easily written in terms of the ϵ^τ_i. In the limit where the mixing reduces to the sole HF configuration, one recovers the standard HF expression for ϵ^τ_i,

$$\epsilon^\tau_i = \langle i_\tau|K|i_\tau\rangle + \sum_{\tau'}\sum_{h=1}^{N^{\tau'}}\langle i_\tau h_{\tau'}|V(\rho)|i_\tau h_{\tau'}\rangle + \frac{1}{2}\sum_{\tau'\tau''}\sum_{h'=1}^{N^{\tau'}}\sum_{h''=1}^{N^{\tau''}}\langle h'_\tau h''_{\tau''}|\frac{\partial V(\rho)}{\partial\rho_{i_\tau i_\tau}}|h'_{\tau'} h''_{\tau''}\rangle. \tag{11}$$

In Eq. (11), summations over h, h', and h'' run over the hole states.

As discussed in Ref. [10], a fully self-consistent solution of the multiconfiguration approach consists of solving simultaneously both Eqs. (5) and (8). It is important to notice that, in our approach, the mean field and beyond mean-field descriptions are obtained in a consistent way since they both follow from variations of the same functional. A standard way to solve both equations is to use an iterative procedure. Starting from a HF solution (characterized by $\rho = \rho_{\rm HF}$ and $\sigma = 0$) that provides an initial set of single particle orbitals, one builds the multiconfiguration basis and solves the configuration mixing Eq. (5). Then, from the mixing coefficients obtained from Eq. (5), one calculates ρ and σ and solves Eq. (8). With the new set of single particle orbitals, one redoes the procedure until convergence of ρ and σ. In this way, the single-particle orbitals contain effects coming not only from the mean field

built with the one-body density matrix ρ but also from the correlations contained in the matrix σ.

In general, the actual solution of Eq. (8) is a very difficult task. In a previous study dedicated to the particular case of pairing-type correlations in the ground states of even-even tin isotopes [10], one has solved Eq. (8) in an approximate way, by neglecting σ. In the present study of even-even silicon isotopes, as a first step, we have solved only the configuration interaction (CI) part [Eq. (5)] of the multiconfiguration approach.

As already pointed out in the Introduction, multiconfiguration methods are able to preserve certain symmetries. Concerning particle numbers, the correlated wave function (2) is a superposition of Slater determinants that conserves exactly the numbers of protons and neutrons. As to angular momentum, the multiconfiguration equations have been solved in the present study only for spherical nuclear configurations, with valence spaces comprising complete spherical subshells. As a consequence, nuclear states have a good total angular momentum J. Actually, since our formalism has been developed in axial symmetry in order to be able to introduce quadrupole deformation explicitly, the only conserved quantum numbers we have are the projection K of the total angular momentum and the parity. The conserved quantum number J is then obtained in the usual manner by performing calculations for successive values $K = 0, 1, 2, \ldots$ and identifying degenerate multiplets. Let us note that the finite axial harmonic oscillator bases used for expanding single-particle states (see below) are defined with a spherical truncation.

III. LOW-LYING STATES IN $^{26-32}$SI

This section is devoted to the description of the low-lying spectroscopy of $^{26-32}$Si using the mp-mh configuration mixing approach. In the first part of this analysis, we investigate the mean-field properties of the ground states provided by the Hartree-Fock-Bogoliubov (HFB) approach using the same D1S Gogny interaction and compare them with the results of a five-dimensional approximate GCM approach.

Technically, the single-particle states introduced in the different approaches (HF, HFB, mp-mh) are expanded onto the harmonic oscillator (HO) bases. In the present work, $N_0 = 11$ major spherical shells have been taken. This basis size has been found sufficient to ensure the convergence of all the results obtained in this work in the three approaches mentioned above. For instance, the convergence of low-lying state energies in the mp-mh configuration mixing approach has been achieved within an accuracy better than 0.1 keV.

A. Ground state deformation properties

In order to investigate the properties of the ground states of $^{26-32}$Si, we start with triaxial HFB calculations constrained according to the dimensionless deformation parameters β and γ,

$$\beta = \frac{\sqrt{5\pi}\sqrt{q_0^2 + 3q_2^2}}{3A^{5/3}r_0^2} \quad \text{and} \quad \gamma = \tan^{-1}\left(\sqrt{3}\,\frac{q_2}{q_0}\right). \quad (12)$$

In Eq. (12), $q_0 = \langle \hat{Q}_0 \rangle = \langle 2z^2 - x^2 - y^2 \rangle$, $q_2 = \langle \hat{Q}_2 \rangle = \langle x^2 - y^2 \rangle$ and $r_0 = 1.2$ fm.

Figure 1 displays the triaxial HFB potential energy surfaces (PES) of $^{26-32}$Si in the β and γ degrees of freedom. Isolines associated with total energy are indicated with a numbering corresponding to the height of the potential (in MeV) relative to the minimum of the HFB potential (dark blue online) for each nucleus. The $\beta_{\rm HFB}$ and $\gamma_{\rm HFB}$ values for the HFB solution of lowest energy are indicated in the second and the third columns of Table I.

From Table I, one sees that the HFB ground states of ^{26}Si and ^{28}Si are similarly characterized by a large value of $\beta_{\rm HFB} \simeq 0.35$ and $\gamma_{\rm HFB} = 60^\circ$. The HFB minima are found to be well deformed on the oblate side. ^{30}Si and ^{32}Si exhibit different characteristics. $\beta_{\rm HFB}$ is equal to zero for ^{30}Si and very close to zero for ^{32}Si. The values of $\gamma_{\rm HFB}$ are very different, $\gamma_{\rm HFB} = 0^\circ$ for ^{30}Si and $\gamma_{\rm HFB} = 34^\circ$ for ^{32}Si. They can be considered as spherical and nearly spherical nuclei, respectively.

Investigating the PESs of Fig. 1, one can deduce that, even though $\beta_{\rm HFB}$ and $\gamma_{\rm HFB}$ may be quite different in the four nuclei, the common feature of the four PESs is their softness in both the β and γ degrees of freedom. In relative, the ^{26}Si PES appears to be more γ soft than the one of ^{28}Si. The PESs of ^{30}Si displays similar features as the one of ^{32}Si. This proposes an important role of triaxiality. This softness is quantitatively evidenced by the mean values $\langle\beta\rangle_{\rm 5DCH}$ and $\langle\gamma\rangle_{\rm 5DCH}$ displayed in Table I. These values have been obtained from a five-dimensional collective Hamiltonian (5DCH) describing both $\beta - \gamma$ and rotation modes with the use of the approach developed in Refs. [9,24]. Let us recall that such an approach is based on the completely microscopic generator coordinate method (GCM) [1] and allows one to find collective excitations of pure rotational-vibrational character from the only data of the nucleon-nucleon effective force. The 5DCH calculations predict strong dynamical β deformations for the ground states of all four silicon isotopes together with significant triaxiality. One observes that the 5DCH collective dynamics introduces considerable changes with respect to HFB in the $\beta - \gamma$ ground state deformations.

To detail the information provided by $\langle\beta\rangle_{\rm 5DCH}$ and $\langle\gamma\rangle_{\rm 5DCH}$ mean values, Fig. 2 shows the 5DCH collective wave functions of $^{26-32}$Si ground states [panels (a), (b), (c), and (d), respectively]. Even though the ^{28}Si collective wave function is partly suppressed for γ between 45 and 60 degrees, the spreading of collective wave functions in $\beta - \gamma$ plane is evident. The spreading in β goes up to $\sim$0.8 for ^{26}Si and ^{28}Si and $\sim$0.6 for ^{30}Si and ^{32}Si.

In Table II we report the energies ϵ_i^τ of the spherical orbitals for $^{26-32}$Si, for protons ($\pi 1d_{5/2}, \pi 2s_{1/2}, \pi 1d_{3/2}$) and neutrons ($\nu 1p_{1/2}, \nu 1d_{5/2}, \nu 2s_{1/2}, \nu 1d_{3/2}, \nu 1f_{7/2}$). These energies slowly evolve from one isotope to the other. We notice a slight increase of the neutron gap between $\nu 2s_{1/2}$ and $\nu 1d_{3/2}$ orbitals in ^{30}Si, which reaches a maximum value of $\simeq$4.56 MeV. A previous study of $N = 16$ isotones with the D1S Gogny interaction have suggested that all $Z = 10$–18 isotones show strong deformations, limiting the understanding of $N = 16$ as a magic number to the sole oxygen neutron drip line [25].

The evolution of proton and neutron single-particle orbitals obtained within the HFB approximation with axial

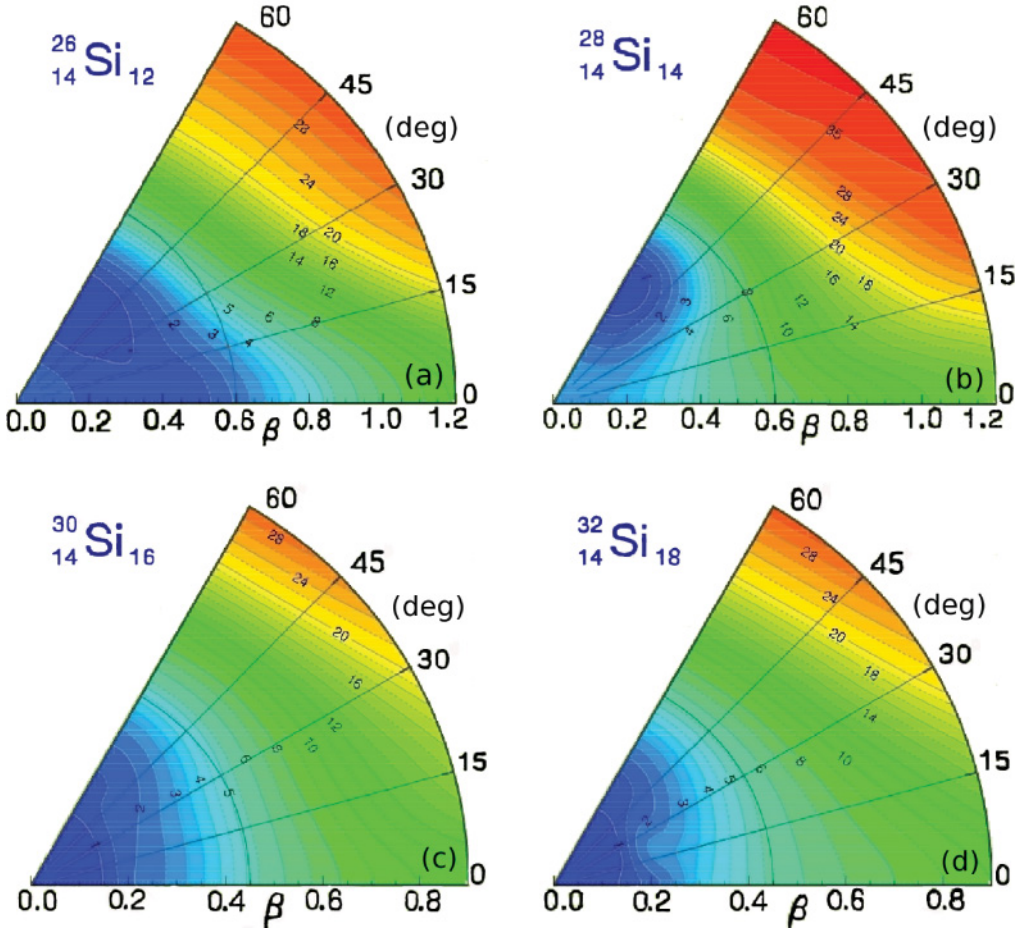

FIG. 1. (Color online) Triaxial HFB potential energy surfaces for $^{26-32}$Si [(a), (b), (c), and (d), respectively] obtained with the D1S Gogny interaction.

deformation β ($\gamma = 0^\circ$) is displayed in Fig. 3. To discuss the general characteristics of single-particle orbitals when spherical symmetry is broken, we have arbitrarily selected the isotopes ^{28}Si (for protons) and ^{32}Si (for neutrons). Open circles (black online), squares (red online), stars (green online), and triangles (blue online) stand for the projections of the angular momentum on the symmetry axis with values $j_z = 1/2, 3/2, 5/2$, and $7/2$, respectively. Solid (dashed) lines correspond to positive (negative) parity orbitals. The chemical potential is indicated with filled black circles and is denoted by λ.

For protons (upper panel), starting from the oblate side and up to the spherical shape, the Fermi level corresponds to the $j_z = 1/2$ deformed orbital originating from the $1d_{5/2}$ shell. From sphericity up to a prolate deformation $\beta \simeq 0.5$, the Fermi level is located on the $j_z = 5/2$ deformed orbital and then migrates to the $j_z = 1/2$ orbital coming from the $2s_{1/2}$ shell; finally, for a very large value of β, it follows the $j_z = 1/2$ deformed orbital coming from the $1f_{7/2}$ shell. The $j_z = 1/2$ and $j_z = 3/2$ deformed orbitals from the $1d_{5/2}$ shell for small oblate deformations fall down instead of going up. Investigating this plot in more detail, one sees that similar trends are encountered for deformed orbitals originated from the $2s_{1/2}$ and $1d_{3/2}$ shells. One is led to the conclusion that these orbitals are strongly mixed through deformation as confirmed by the presence of avoided level crossings in single-particle spectra. The natural continuity of the oblate $j_z = 1/2$ from the $1d_{5/2}$ shell is the prolate $j_z = 1/2$ from the $1d_{3/2}$ shell. Other examples are the oblate $j_z = 1/2$ from the $2s_{1/2}$ shell and the prolate $j_z = 1/2$ from the $1d_{5/2}$ shell, the oblate $j_z = 1/2$ level from the $1d_{3/2}$ shell and the prolate $j_z = 1/2$ from the $2s_{1/2}$ shell, or the oblate/prolate $j_z = 3/2$ from the $1d_{5/2}$ shell and the prolate/oblate $j_z = 3/2$ from the $1d_{3/2}$ shell. From this kind of analysis, one expects that the proton excitations contributing to low-lying states will mainly arise from the sd shell, while the influence of the $j_z = 1/2$ level from the $1f_{7/2}$ shell will appear only at quite large β deformation. It is important to note

TABLE I. β and γ deformation properties of the $^{26-32}$Si ground states from the HFB and 5DCH approaches and the D1S Gogny interaction.

Nucleus	β_{HFB}	γ_{HFB}	$\langle\beta\rangle_{\mathrm{5DCH}}$	$\langle\gamma\rangle_{\mathrm{5DCH}}$
^{26}Si	0.32	60.0°	0.41	28°
^{28}Si	0.37	60.0°	0.40	27°
^{30}Si	0.00	0.0°	0.39	29°
^{32}Si	0.01	34.0°	0.37	28°

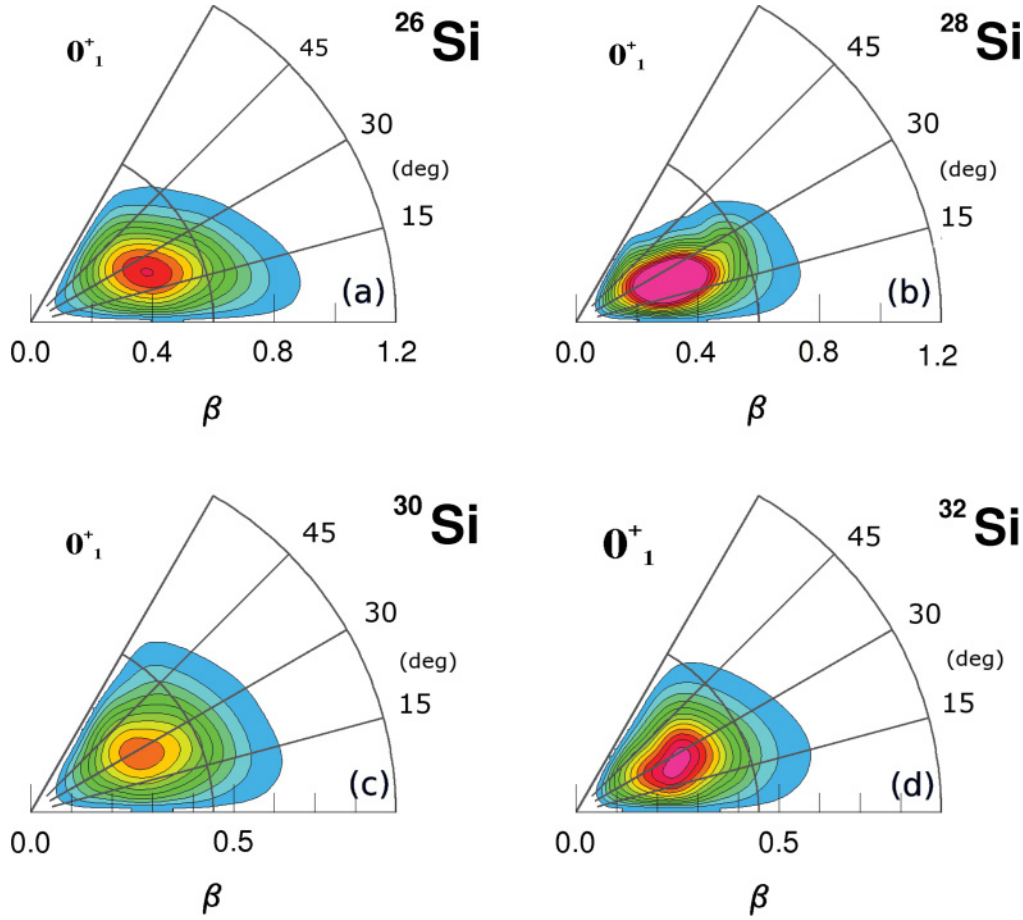

FIG. 2. (Color online) Ground state 5DCH collective wave functions for $^{26-32}$Si [(a), (b), (c), and (d), respectively].

that these mixings and repulsions of deformed orbitals are not necessarily synonymous with inversions of orbitals.

The behavior of the neutron orbitals is similar. As in the present paper we study isotopes where the $2s_{1/2}$ and $1d_{3/2}$ neutron subshells are filled or partially filled, it is important to look at higher shells. Here we only mention that the same game as for protons is played between deformed neutron orbitals originating from $1f_{7/2}$, $2p_{3/2}$, and $2p_{1/2}$ with low j_z values, see Fig. 3(b), and that upper shells of negative parity play a role at small deformations only for the heavier isotopes.

B. Low-lying spectroscopy

In this subsection we discuss the low-lying states in the even-even $^{26-32}$Si isotopes as predicted by the mp-mh configuration mixing approach and compare them with the ones obtained with the 5DCH method. Only positive parity states are investigated in this work. Experimentally, these nuclei are challenging as they exhibit a large variety of states at low energy, and strong changes arise from one isotope to another (for example, in the 2^+_2 state). For this reason, from the theoretical viewpoint, they can be considered as benchmarks for both the many-body method employed and the properties of the effective nucleon-nucleon interaction used. The comparison with the 5DCH approach, a method that has proved its pertinence through a global survey [9], is interesting in the sense that, as the same D1S Gogny interaction is used, it enables one to specify the role of rotational and quadrupole correlations in the spectroscopy of the positive parity states in silicon isotopes.

TABLE II. Energies (in MeV) of spherical proton and neutron HFB single-particle states in $^{26-32}$Si.

	$\pi d_{5/2}$	$\pi s_{1/2}$	$\pi d_{3/2}$	$\nu p_{1/2}$	$\nu d_{5/2}$	$\nu s_{1/2}$	$\nu d_{3/2}$	$\nu f_{7/2}$
^{26}Si	−7.07	−2.61	0.88	−27.73	−15.96	−10.73	−7.33	−1.37
^{28}Si	−10.05	−5.16	−1.69	−28.39	−15.95	−10.91	−7.34	−1.18
^{30}Si	−12.60	−7.32	−4.11	−26.75	−16.21	−11.56	−7.29	−1.41
^{32}Si	−15.09	−10.08	−7.51	−26.44	−16.28	−11.40	−7.80	−2.01

All the mp-mh results we present below correspond to mixing within the sd shell. We have checked the influence on the low-lying states of our interest when including the $1p$ and $1f$ subshells. In particular, the adding of $1p_{1/2}$ and $1p_{3/2}$ had essentially no effect on the spectroscopy of ^{26}Si, ^{28}Si, ^{30}Si, and ^{32}Si. For the selected spectroscopy of ^{26}Si, the effect of the $1f_{7/2}$ shell was very small. For ^{28}Si, only small variations were observed and they concerned only the highest states. The largest differences ($\sim$500 keV) due to the $1f_{7/2}$ and $2p_{3/2}$ orbitals have been encountered in ^{30}Si and ^{32}Si. Concerning the 5DCH approach, only theoretical results with energies lower than $\simeq$12 MeV are presented. This choice is not fully arbitrary as it is motivated by the relative maximum height of PESs

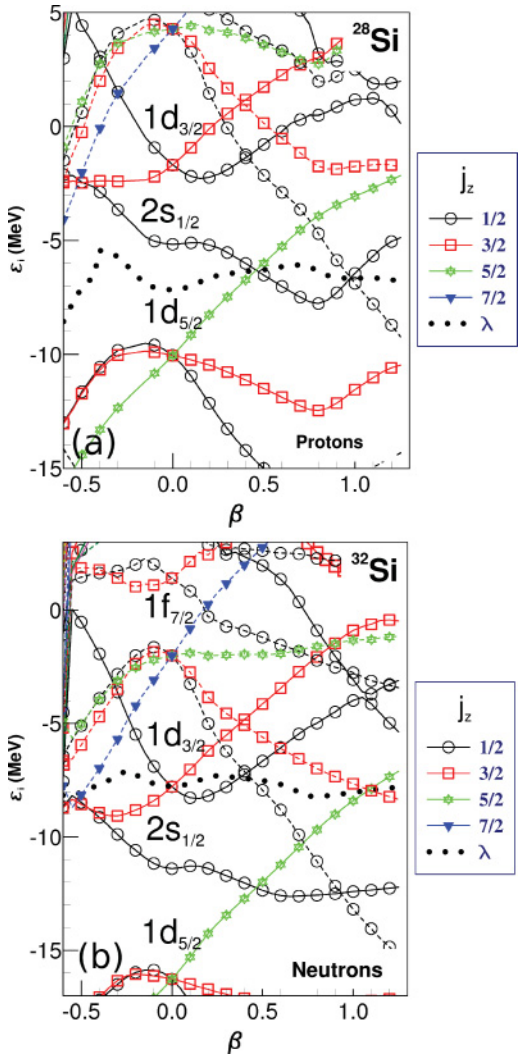

FIG. 3. (Color online) Evolution of proton and neutron single-particle orbitals obtained within the HFB approximation with the axial deformation β ($\gamma = 0^\circ$) in ^{28}Si (a) and ^{32}Si (b).

($\simeq$ 28 MeV above the HFB minimum in the present case, see Fig. 1) used to perform the GCM configuration mixing of nuclear shapes.

For the four isotopes, 3^- is the lowest negative parity state. Its experimental energy is 6.789 MeV in ^{26}Si, 6.879 MeV in ^{28}Si, 5.487 MeV in ^{30}Si, and 5.288 MeV in ^{32}Si. The decrease of its value gives a flavor of the increasing importance of negative parity orbitals at low energy in ^{30}Si and ^{32}Si. However, for the description of positive parity states, negative parity orbitals should play a role at energies higher than for the description of negative parity states as one has to introduce at least 2p-2h excitations to produce a positive parity state.

Excitation energies calculated with the mp-mh and 5DCH methods for $^{26-32}$Si are compared to experimental values in Tables III–VI (the energies are expressed in MeV). In Table V, a sixth column named mp-mh$_s$ has been added, showing mp-mh results shifted by 2.5 MeV. Positive parity has been assumed for the states in ^{26}Si whose spins are not assigned experimentally, based on the plausible hypothesis

TABLE III. Excitation energies (in MeV) of positive parity low-lying states in ^{26}Si from experiments (second column), and calculated with the variational mp-mh configuration mixing method using the D1S Gogny force (third column). In the fourth column a few energies derived from the 5DCH approach [9] are displayed. The asterisk means that the spin of the state is not experimentally assigned. The question mark indicates a state which is not seen experimentally.

Nucleus	States	Experiment	mp-mh	5DCH
^{26}Si				
	2_1^+	1.795	1.502	2.426
	2_2^+	2.783	2.567	5.124
	0_2^+	3.332	3.740	8.146
	3_*^+	3.756	3.233	9.126
	4_*^+	3.842	3.293	6.119
	3_*^+	4.093	3.779	
	2_3^+	4.138	3.915	
	4_*^+	4.183	4.758	9.254
	2_*^+	4.446	4.783	
	0_3^+	4.806	4.959	
	4_*^+	5.229	4.931	
	4_1^+	5.330	5.741	
	2_*^+	5.562	5.577	
	$3_?^+$	?	5.755	
	0_4^+	5.940	6.690	
	2_4^+	6.350	6.823	

that the lowest negative parity state is the observed 3^- one. The question mark means that the state is not observed experimentally. For ^{28}Si, the asterisk indicates that both spin and parity have not been measured experimentally; again, making the assumption of positive parity, the spin is given by our model. For ^{32}Si, because of the energy of the lowest observed 3^- state, positive parity is assumed for the fourth state at 5.220 MeV. Experimentally, the spin is expected to be in the range from 1 to 4; our model predicts spin 3. Concerning the 4_*^+ state, the experimental assignment is either 4^+ or 5^-.

Theoretical results are provided for $\sim$20 states in each isotope, except for ^{32}Si where the spin and parity of some states with excitation energies larger than $\sim$5.5 MeV have not been firmly assigned experimentally. All excited configurations from the sd shell have been introduced in the mp-mh wave functions, up to 6p-6h on the proton side and 2p-2h, 4p-4h, 6p-6h on the neutron side depending on the isotopes. Then, the presented results contained up to 10p-10h configurations in ^{26}Si and ^{30}Si, 12p-12h configurations in ^{28}Si, and 8p-8h configurations in ^{32}Si.

In the case of ^{26}Si, one sees that there is a very good agreement between experimental and mp-mh configuration mixing energies, whatever the spin and the excitation energy. Concerning the 5DCH approach, the energy of the 2_1^+ state is found too high by $\sim$700 keV and the energies of the other excited states are also strongly overestimated (by several MeV). In the case of ^{28}Si, despite the inversion between the 4_1^+ and 0_2^+ levels, quite good agreement with experiment is obtained by the mp-mh approach. Again, the 5DCH approach tends to overestimate excitation energies. However, we note

TABLE IV. Same as Table III for ^{28}Si; The asterisk means that spin-parity quantum numbers are not assigned experimentally.

Nucleus	States	Experiment	mp-mh	5DCH
^{28}Si				
	2_1^+	1.779	1.993	2.469
	4_1^+	4.618	5.372	6.446
	0_2^+	4.980	4.409	10.591
	3_1^+	6.276	6.365	
	0_3^+	6.690	8.760	
	4_2^+	6.888	7.769	
	2_2^+	7.381	7.280	7.395
	2_3^+	7.416	8.353	
	3_2^+	7.799	8.124	
	2_4^+	7.933	8.551	
	2_5^+	8.259	9.025	
	1_1^+	8.328	8.943	
	6_1^+	8.544	9.531	11.876
	3_3^+	8.589	8.459	
	0_*^+	8.819	9.345	
	5_1^+	8.945	9.424	
	0_*^+	8.953	9.845	
	4_3^+	9.164	10.120	
	3_4^+	9.315	9.894	
	2_6^+	9.381	9.883	
	4_4^+	9.417	10.719	
	2_7^+	9.479	9.952	
	1_2^+	9.496	9.756	

that both theoretical approaches describe the 2_1^+ state within the same accuracy as in ^{26}Si and that the energy of the 2_2^+ state is particularly well reproduced.

In ^{30}Si, as seen from Table V, the energy of the 2_1^+ is overestimated by ∼2.5 MeV with the mp-mh configuration

TABLE V. Same as Table III for ^{30}Si.

Nucleus	States	Experiment	mp-mh	5DCH	mp-mh$_s$
^{30}Si					
	2_1^+	2.235	4.609	2.222	2.109
	2_2^+	3.498	5.704	4.729	3.208
	1_1^+	3.769	6.338		3.838
	0_2^+	3.788	7.732	7.610	5.238
	2_3^+	4.810	8.230	11.832	5.730
	3_1^+	4.831	6.709	8.056	4.209
	3_2^+	5.231	7.904		5.404
	4_1^+	5.279	7.539	5.691	5.039
	0_3^+	5.372	8.950	8.585	6.450
	2_4^+	5.614	9.262		6.762
	4_2^+	5.950	8.911	8.714	6.441
	2_5^+	6.538	10.186		7.686
	0_4^+	6.642	9.030		6.530
	3_3^+	6.865	8.831		6.331
	2_6^+	6.914	10.594		8.094
	5_1^+	6.998	10.926		8.426

TABLE VI. Same as Table III for ^{32}Si. The asterisk indicates that spin and/or parity are/is not assigned experimentally.

Nucleus	States	Experiment	mp-mh	5DCH
^{32}Si				
	2_1^+	1.941	1.959	2.215
	2_2^+	4.230	4.871	5.014
	0_2^+	4.984	6.810	5.318
	3_*^+	5.220	6.004	
	2_3^+	5.412	6.758	9.335
	4_*^+	5.502	6.567	5.470

mixing. What is even more surprising is that all states appear to be shifted upward. Actually, reduction of all the excitation energies by ∼2.5 MeV gives a much better agreement with experiment. This can be seen from the last column "mp-mh$_s$" of Table V that gives the values provided by the mp-mh configuration mixing approach minus 2.5 MeV. Then, the discrepancy with experiment is reduced to ∼0.69 MeV (on average), and the theoretical level sequence becomes very similar to the experimental one. We have checked that this global shift cannot be removed by adding the $1f_{7/2}$ shell to the valence space. Its origin will be discussed later in this subsection.

On the other hand, the energies of several states in this nucleus are well reproduced by the 5DCH approach, in particular those of the 2_1^+ and 4_1^+ states. Let us note in this respect that the 5DCH method does not explicitly make use of the matrix elements of the residual interaction between excited configurations, exploiting instead the quadrupole deformation properties of the mean field. As seen and discussed in relation to Fig. 3, following the chemical potential, the deformation is able to catch part of the correlation information coming from upper spherical shells directly or through the mixing of deformed orbitals (see discussion in Sec. III A on the evolution of single-particle orbitals). In the case of ^{32}Si, both theoretical methods provide a good description of the selected experimental states (except for the 0_2^+ with the mp-mh configuration mixing method and the 2_3^+ with the 5DCH approach).

The results obtained with the mp-mh configuration mixing indicate that this approach is capable of reproducing quite well the low-energy spectroscopy of ^{26}Si and ^{28}Si and to a lesser extent, the one of ^{32}Si. The mean deviations between theory (mp-mh) energies and experimental ones are found to be ∼369 keV in ^{26}Si, ∼653 keV in ^{28}Si and ∼946 keV in ^{32}Si. The increase of the deviation between ^{26}Si and ^{28}Si can be attributed to the systematic overestimation obtained in the calculation of ^{28}Si highest levels. The same phenomenon holds for ^{32}Si. As pointed out previously, this effect can be partly ascribed to the absence of the $1f_{7/2}$ shell, and, to a smaller extent, of the $2p_{3/2}$ shell in the present calculations. Nonetheless, the agreement with experiment of mp-mh energies can be considered as rather encouraging, considering the fact that the D1S Gogny interaction has not been devised to describe the kind of general correlations introduced in a multiconfiguration approach. In particular, the proton-neutron matrix elements between excited configurations given by this interaction have not been constrained.

The following discussion is dedicated to the understanding of the origin of the shift obtained with the mp-mh configuration mixing method for excited states in ^{30}Si. In a schematic way, both energy gaps between single-particle orbitals and coupling matrix elements (ME) between configurations are the key quantities that drive the low-lying spectroscopy. One can infer that a downward shift can be obtained either by decreasing gaps (an effect similar to the monopole shifts pointed out in the shell model approach [26–28]), and/or by varying coupling matrix elements. Proton-neutron matrix elements are suspected to be mainly responsible for the energy shift encountered in ^{30}Si. In fact, by changing "by hand" the values of selected proton-neutron ME implying the spin-orbit partners $1d_{3/2}$ and $1d_{5/2}$ and using them in realistic mp-mh configuration mixing calculations (which produces a modification of the energy of the $1d_{3/2}$ shell), one can derive excited states in ^{30}Si which are in reasonably good agreement with experiment, with deviations similar to the ones found in ^{28}Si. It is important to note that such changes in matrix elements essentially effect only the ^{30}Si spectrum. In particular no significant modification of ^{28}Si spectrum is observed. In addition, as we will see in Sec. IV where the chaotic behavior of highly excited Slater determinants is studied, too strong couplings are found essentially in $K = 0$ cases, where common proton-neutron matrix elements are involved.

At this stage of our analysis, one has to recall that the general formalism of the mp-mh configuration mixing method exposed in Sec. II implies that not only the secular equation (5) has to be solved but also Eq. (8). These two equations in principle provide the "best" single-particle representation, i.e., the one that minimizes the total energy consistent with correlations. Clearly, the solution of Eq. (8) may introduce modifications on both single-particle energies and coupling ME. However, discussing the kind of renormalization produced by Eq. (8) is far beyond the scope of the present paper, and it will be left to a dedicated study. Let us simply mention here that, in the context of the present work, introducing a tensor term in the effective interaction we would probably reproduce the right energy evolution of spin-orbit partners [29]. In addition, a crude comparison between sd-shell ME calculated from the D1S Gogny interaction and from the USD interaction used in the shell model [30] displays large discrepancies essentially in the $T = 0$ channel, where the renormalization effects are expected to be the largest. The average difference is equal to ∼0.3 MeV in $T = 1$ channel and ∼1.5 MeV in $T = 0$ one. The large difference found in $T = 0$ channel is attributed essentially to two ME and comes from the lack of tensor term by comparing the different contributions to ME (central, spin-orbit and tensor).

In conclusion of this part, one can say that, in the four silicon isotopes, most states contain more complex correlations than the usual collective quadrupole/rotational ones. In order to identify the nature of the ground state band, we have calculated the energy ratio $(4_1^+/2_1^+)$ whose value is a standard indicator of the vibrational, rotational, or γ-soft nature of nuclei. Results for experiment, mp-mh configuration mixing and 5DCH methods are displayed in Fig. 4. Numerical values are reported in Table VII for experiment, mp-mh configuration mixing, and 5DCH methods. From experiment, one observes that ^{26}Si is close to the vibrational limit $[(4_1^+/2_1^+)_{\rm vib} = 2]$, while ^{28}Si and ^{30}Si are more γ-soft nuclei $[(4_1^+/2_1^+)_{\gamma} = 2.5]$. In ^{32}Si, this ratio increases toward the rotor limit $[(4_1^+/2_1^+)_{\rm rot} = 3.3]$. The results obtained with the mp-mh configuration mixing show that data in ^{26}Si and ^{28}Si are well reproduced and display the experimental trend. For ^{30}Si, the shifted values for the mp-mh configuration mixing approach have been used. The significant overestimation in ^{32}Si, where the 2_1^+ energy is well reproduced, comes from the fact that the 4_1^+ energy is slightly overestimated.

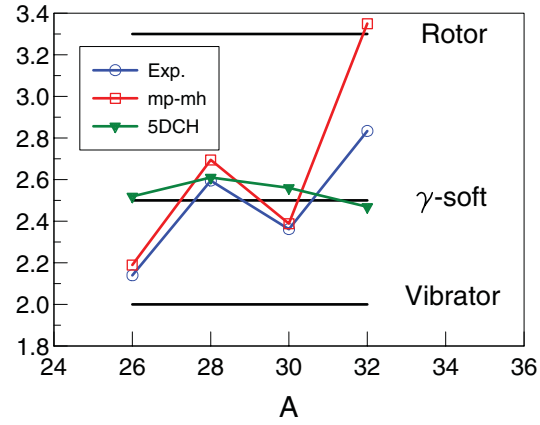

FIG. 4. (Color online) Experimental and calculated (mp-mh and 5DCH) $E(4_1^+)/E(2_1^+)$ ratios. For ^{30}Si, the shifted for mp-mh configuration mixing energies have been used (see text).

C. Role of the proton-neutron residual interaction

This part discusses the role of the proton-neutron residual interaction and the importance of using an effective nucleon-nucleon interaction that manifests good properties in the $T = 0$ channel when using mp-mh configuration mixing methods. As a benchmark nucleus, we have chosen ^{28}Si. Table VIII lists the first seven excited states of ^{28}Si. The experimental values of excitation energies and the theoretical ones (mp-mh) are given in columns 2 and 3. Columns 4 and 5 display the results obtained within the mp-mh configuration mixing approach when the residual proton-neutron interaction is turned off. As the Hamiltonian in use is not exactly isospin-invariant (a Coulomb term is included), this symmetry breaking leads to a small difference (less than ∼300 keV) for proton and neutron solutions, noted mp-mh$_\pi$ and mp-mh$_\nu$, respectively.

TABLE VII. Numerical values of experimental and calculated (mp-mh and 5DCH) $E(4_1^+)/E(2_1^+)$ ratios. The superscript "s" for mp-mh ratios in ^{30}Si means that the energies shifted by 2.5 MeV have been used, see text.

Nucleus	$\frac{E(4_1^+)}{E(2_1^+)}_{\rm exp.}$	$\frac{E(4_1^+)}{E(2_1^+)}_{m\text{-}mh}$	$\frac{E(4_1^+)}{E(2_1^+)}_{\rm 5DCH}$
^{26}Si	2.140	2.190	2.520
^{28}Si	2.595	2.695	2.611
^{30}Si	2.362	2.389^s	2.561
^{32}Si	2.834	3.350	2.469

TABLE VIII. Excitation energies (in MeV) of low-lying states in ^{28}Si calculated with the variational mp-mh configuration mixing method with and without residual proton-neutron interaction (see text).

States	Experiment	mp-mh	mp-mh$_\pi$	mp-mh$_\nu$
2_1^+	1.779	1.993	5.733	5.831
4_1^+	4.618	5.372	6.553	6.712
0_2^+	4.980	4.409	9.588	9.651
3_1^+	6.276	6.365	9.732	?
0_3^+	6.690	8.759	9.873	9.893
4_2^+	6.888	7.769	?	?
2_2^+	7.380	7.280	10.283	10.415

The sensitivity of the excitation energies to the proton-neutron residual interaction depends on the nature of states. For example, this interaction brings the energy of the 2_1^+ state from ∼6 MeV to ∼2 MeV; its importance for the structure of correlated wave functions is illustrated in Table IX where the components of the wave functions of the 0_1^+ and 0_2^+ states are listed in two cases. We define the quantity W_n that measures the correlation content of the wave functions in terms of the order of excitation n, namely 0p-0h, 1p-1h, 2p-2h, ... For a given eigenfunction $|\Psi_\beta\rangle$,

$$W_n^\beta = \sum_{k_n} \left|A_{k_n}^\beta\right|^2, \tag{13}$$

where k_n represents the Slater determinant components with np-nh excitations ($n = n_\pi + n_\nu$). Case (a) in Table IX corresponds to a full calculation and case (b) to a calculation without residual proton-neutron interaction. The wave functions 0_1^+ and 0_2^+ have quite different structures. For the ground state, excited 2p-2h configurations play a role as important as the initial 0p-0h configuration. When the proton-neutron residual interaction is turned off, most of the correlations disappear. One sees that the 2p-2h configurations built from 1p-1h proton excitations combined with 1p-1h neutron excitations are essential for the description of the ground state. For the excited state, the absence of proton-neutron interaction is even worse as it destroys fully the 0p-0h component and produces the solutions based on a 1p-1h proton or on a 1p-1h neutron configuration. One observes that the proton-neutron interaction brings a lot of fragmentation in the wave functions,

TABLE IX. Weights W_n ($n \leqslant 8$) calculated for 0_1^+ and 0_2^+ states in ^{28}Si. Case (a) corresponds to the full mp-mh calculation and case (b) to a calculation without residual proton-neutron interaction. The index π (ν) specifies the proton (neutron) solution.

State	Case	W_0	W_1	W_2	W_3	W_4	W_5	W_6	W_7
0_1^+	(a)	34.48	0.00	34.77	11.55	12.78	4.25	1.76	0.34
	(b)	93.77	0.00	6.03	0.02	0.17	0.00	0.00	0.00
0_2^+	(a)	43.70	0.00	12.26	14.12	16.37	8.68	3.82	0.90
	(b_π)	0.00	91.51	2.82	5.34	0.20	0.12	0.00	0.00
	(b_ν)	0.00	91.39	3.25	5.04	0.21	0.11	0.00	0.00

TABLE X. Proton and neutron occupation probabilities of the $d_{5/2}$, $s_{1/2}$, and $d_{3/2}$ orbitals, for 0_1^+ and 0_2^+ states in ^{28}Si. Case (a) corresponds to a full calculation and case (b) to a calculation without residual proton-neutron interaction.

State	Case	$\pi d_{5/2}$	$\nu d_{5/2}$	$\pi s_{1/2}$	$\nu s_{1/2}$	$\pi d_{3/2}$	$\nu d_{3/2}$
0_1^+	(a)	5.053	5.047	0.603	0.606	0.344	0.347
	(b)	5.939	5.932	0.018	0.020	0.043	0.047
0_2^+	(a)	4.960	4.978	0.716	0.698	0.324	0.324
	(b_π)	4.941	5.912	1.007	0.037	0.050	0.050
	(b_ν)	5.935	4.935	0.033	1.008	0.046	0.057

hence collectivity. The precise knowledge of this residual interaction is therefore mandatory in mp-mh configuration mixing approaches, in particular when calculations are performed at sphericity. Consistently with the results for the wave functions, occupation probabilities display strong changes as can be seen in Table X in the case of proton and neutron $1d_{5/2}$, $2s_{1/2}$, and $1d_{3/2}$ orbitals.

IV. STATISTICAL PROPERTIES OF HIGHLY EXCITED CONFIGURATIONS

One of the main issues raised by multiconfiguration approaches is the number of relevant configurations for describing low-lying states. Because of the proton-neutron excitations, this number can rapidly explode. In realistic calculations, one has to think about truncations based on physical arguments. When going beyond the mean-field with the mp-mh approach, it is assumed that short-range correlations have already been taken into account through the effectiveness of the nucleon-nucleon interaction used (the D1S Gogny interaction in our case). Our aim is to treat explicitly the long-range correlations corresponding to the attractive part of the nucleon-nucleon interaction. Two standard types of truncation can be proposed, independently of the choice (or not) of a valence space: a truncation on the order of the excitations and/or a truncation on the configuration excitation energies. Both types of truncations seem to be reasonable in the present context. In order to define appropriate truncations based on relevant physics argument, we discuss below the behavior of highly excited configurations.

We have followed the direction used in Refs. [12–16] where the analysis was based on the properties of the strength function associated with the Slater determinants. Using second quantization and the standard Wick's theorem decomposition, the Hamiltonian $\hat{\mathcal{H}}$, Eq. (6), is the sum of an independent particle part $\hat{\mathcal{H}}_0$ (one-body) and a residual part $\hat{\mathcal{H}}'$ (one-body and two-body),

$$\hat{\mathcal{H}} = \hat{\mathcal{H}}_0 + \hat{\mathcal{H}}'. \tag{14}$$

The eigenfunctions $|k\rangle$ of the unperturbed Hamiltonian $\mathcal{H}_0$,

$$\mathcal{H}_0|k\rangle = \epsilon_k|k\rangle, \tag{15}$$

describe noninteracting fermions. In the basis $|k\rangle$, the residual interaction $\hat{\mathcal{H}}'$ has both diagonal, $\overline{\hat{\mathcal{H}}}$, and off-diagonal, $\widetilde{\hat{\mathcal{H}}}$, matrix elements: $\hat{\mathcal{H}}' = \overline{\hat{\mathcal{H}}} + \widetilde{\hat{\mathcal{H}}}$. Full diagonalization leads to

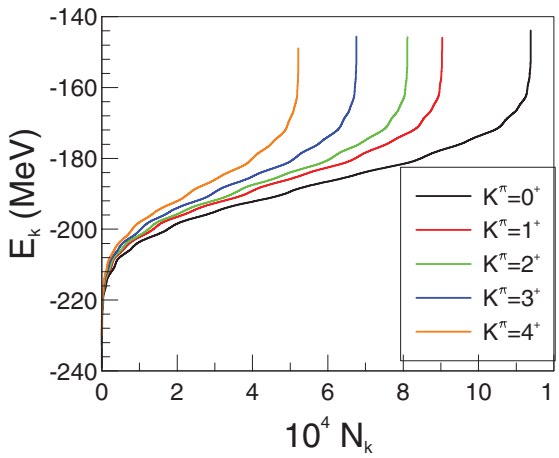

FIG. 5. (Color online) Centroid energies (in MeV) for ^{28}Si. The x axis corresponds to the number of centroids ordered by increasing energies.

the stationary states $|\alpha\rangle$ and their energies $\mathcal{E}_\alpha$,

$$\hat{\mathcal{H}}|\alpha\rangle = \mathcal{E}_\alpha|\alpha\rangle. \tag{16}$$

The eigenfunctions $|\alpha\rangle$ may have a complicated structure in the original basis $|k\rangle$,

$$|\alpha\rangle = \sum_k A_k^\alpha |k\rangle. \tag{17}$$

where A is a unitary matrix:

$$\sum_k A_k^\alpha A_k^{\alpha'} = \delta^{\alpha\alpha'}, \sum_\alpha A_k^\alpha A_{k'}^\alpha = \delta_{kk'}. \tag{18}$$

A completely delocalized wave function $|\alpha\rangle$ would have a number of relevant components close to the total dimension N of the multiconfiguration space (for given exact quantum numbers). In this limit the typical magnitude of each component is $1/\sqrt{N}$. In general, a number N_α of principal components $|k\rangle$ characterizes the delocalization of a state $|\alpha\rangle$ in the given basis (15). Indeed, a two-body interaction cannot couple configurations differing by more than two particle states which implies a band-like Hamiltonian matrix, favoring the localization of eigenfunctions in the Hilbert space. Conversely, the fragmentation of simple basis states over the energy spectrum can be provided by the strength function defined by the quantity

$$F_k(E) = \langle k|\delta(E - \hat{H}(\rho))|k\rangle = \sum_\alpha \left|A_k^\alpha\right|^2 \delta(E - \mathcal{E}_\alpha). \tag{19}$$

The strength function contains rich information but requires the knowledge of the full nuclear spectrum. Fortunately, one can study the main characteristics of the system from the first and the second moment of the strength function which does not require the actual diagonalization of $\mathcal{H}$. These two moments are the centroid, E_k, and dispersion, σ_k, of the state distribution,

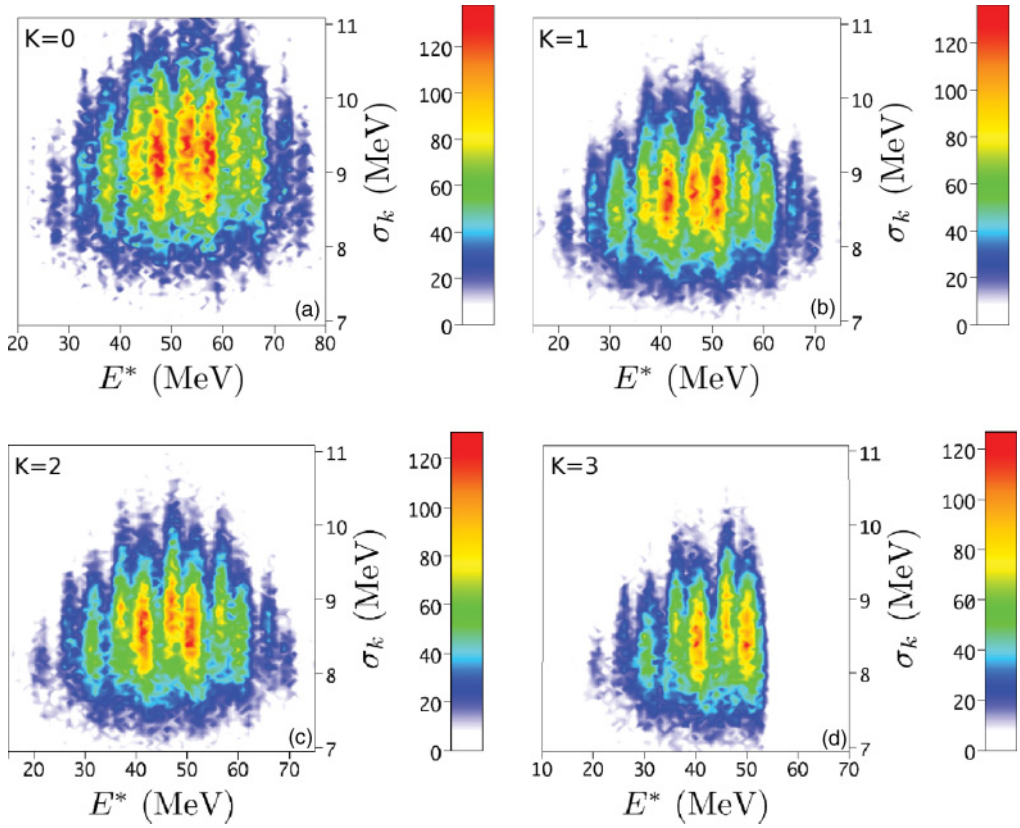

FIG. 6. (Color online) Dispersions σ_k (in MeV) of $K^\pi = 0^+, 1^+, 2^+$, and 3^+ Slater determinants for ^{28}Si. The x axis represents the excitation energies E^* of Slater determinants. The color code indicates the number of Slater determinants per bins of excitation energy and dispersion.

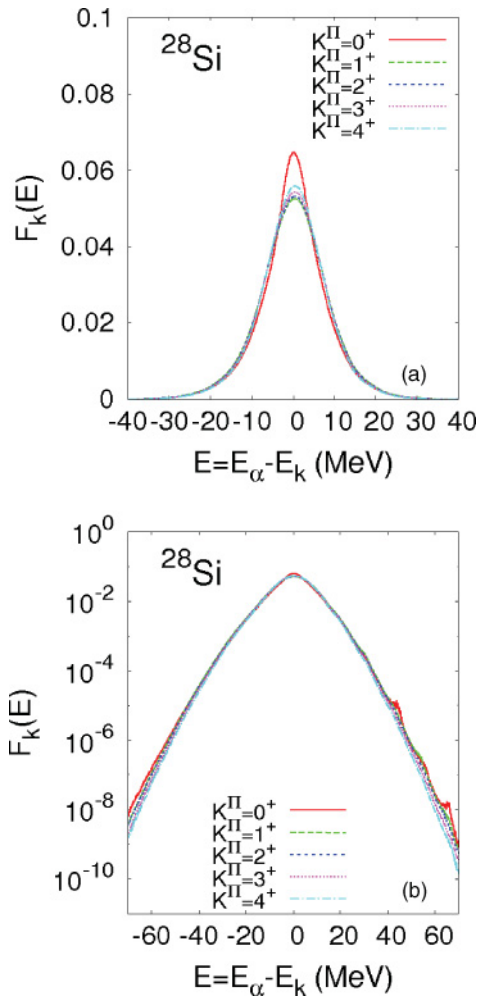

FIG. 7. (Color online) The ^{28}Si strength functions associated with $K^\pi = 0^+$, 1^+, 2^+, 3^+, and 4^+ components in linear scale (upper panel) and logarithmic scale (lower panel). Logarithmic representation is shown in lower panel. Calculations have been performed with a 0.1 MeV bin.

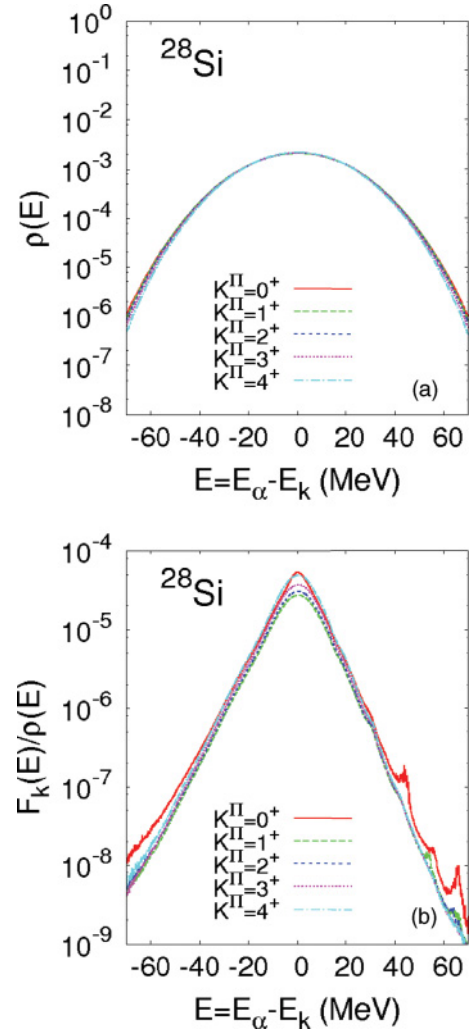

FIG. 8. (Color online) The ^{28}Si Slater determinant distributions $\rho(E)$ (upper panel) and the ^{28}Si locally normalized strength functions $\langle F_k(E)\rangle/\rho(E)$ (lower panel) for $K^\pi = 0^+$, 1^+, 2^+, 3^+, and 4^+ components. Calculations have been performed with a 0.1 MeV bin.

given by

$$E_k = \int dE E F_k(E) = \mathcal{H}_{kk} = \epsilon_k + \overline{\mathcal{H}}_{kk}, \tag{20}$$

and

$$\sigma_k^2 = \int dE (E - \overline{E}_k)^2 F_k(E) = \sum_{l(\neq k)} (\mathcal{H}'_{lk})^2, \tag{21}$$

respectively. The centroid $\overline{E}_k$ coincides with the unperturbed energy $\mathcal{H}_{kk}$, whereas the dispersion depends only on the off-diagonal matrix elements $\mathcal{H}'_{lk}$.

Below we discuss the example of the ^{28}Si isotope. Similar calculations have been done for other nuclei with similar conclusions. At this point, it is important to recall that the mp-mh configuration mixing formalism presented in Sec. II has been developed, in practice, using an axially deformed harmonic oscillator basis. In order to preserve the spherical symmetry, all the mp-mh calculations displayed in this study have been done for $\beta = 0$. In the following, our analysis is done in terms of different projections K of a given angular momentum J. All configurations of the sd shell (up to 12p-12h) have been introduced in the wave functions; the maximum size of the Hamiltonian matrices that have been fully diagonalized was $\sim$90 000 $\times$ 90 000.

Figure 5 displays the values of the centroid energies E_k, where centroids are labeled by N_k and ordered by increasing energy. One observes a characteristic behavior for all values of K from 0 to 4. The lowest centroid energy, the one associated with the 0p-0h configuration, is -239.203 MeV. Only few configurations have small excitation energy. The level density increases rapidly with excitation energy, and most configurations are located in the range $[-210; -160]$ MeV. The final increase, beyond -160 MeV, is an artifact of the finite valence space that reduces the number of possible highly excited states.

Figure 6 shows the dispersions σ_k of Eq. (21) for all configurations characterized by $K = 0, 1, 2$, and 3 and their excitation energies E^* (in MeV). The color code indicates

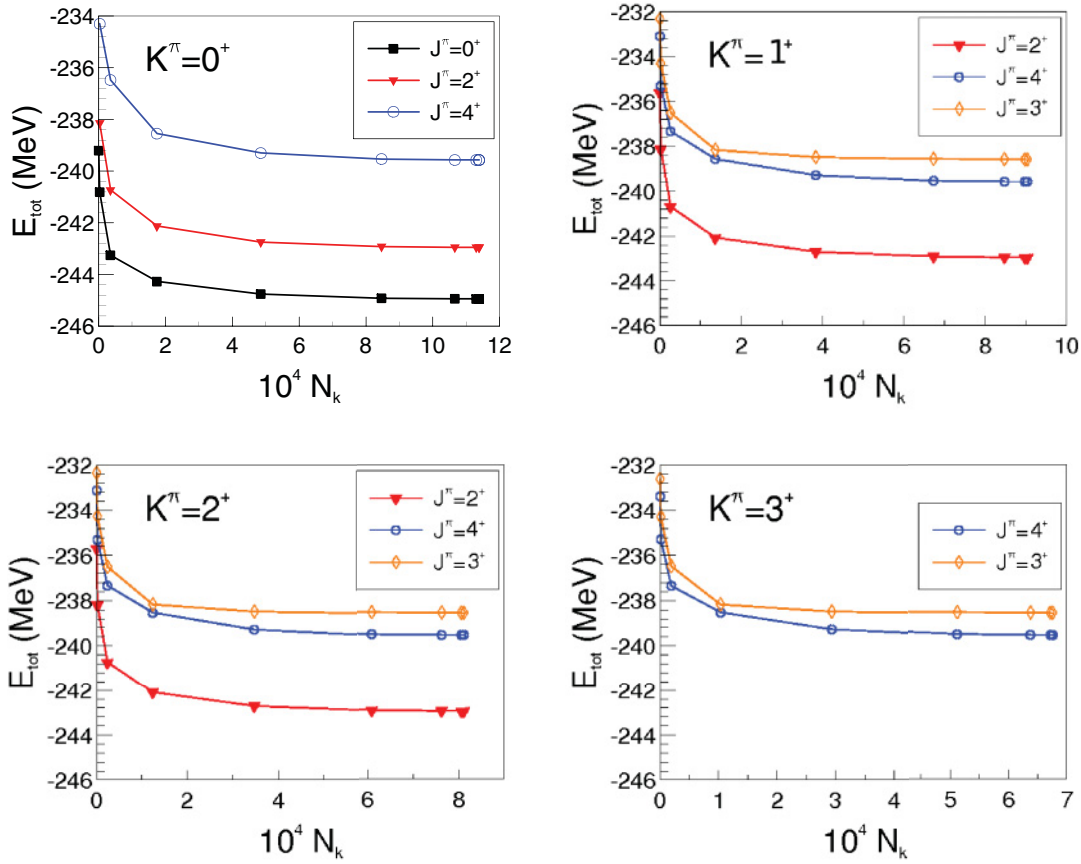

FIG. 9. (Color online) Convergence of ground state and a few excited state energies in ^{28}Si as a function of the number of configurations ordered by their centroid energies.

the number of configurations in a given excitation energy and σ_k bin. As expected, the structure of the configuration distribution is different for different values of K but most configurations are concentrated along a central line, and characteristic structures appear in the most dense areas. Such areas are more pronounced in the most dense zone in the $K = 0$ case for all values of E^*. A large majority of configurations display a dispersion σ_k that is rather constant along the spectrum; its mean value can be evaluated to be $\sim$9 MeV. This important result which implies that strength functions can be characterized by essentially the same width is the first indication of expected exponential convergence.

The strength function of ^{28}Si is presented in Fig. 7 for different values of K as a function of the energy counted from the corresponding centroid, $E_\alpha - E_k$. The value of the bin is set to 0.1 MeV. An average over all configurations has been done in order to reveal possible generic behavior. The upper panel displays the strength function in linear scale and the lower panel in logarithmic scale. The central part of the distribution is intermediate between a Gaussian and a Lorentzian one, whereas the behavior in the wings is found to be a decreasing exponential. This is clearly visible in the logarithmic scale. In agreement with [12–16], the coupling of highly excited configurations with low-energy eigenfunctions therefore exhibits an exponential regime and the "3σ" rule characterizing the start of the exponential convergence, which is important in practical calculations of the level density by methods of statistical spectroscopy [31], seems to hold here also.

In the case of the $K = 0$ projection, one observes two unusual bumps at energies $E_\alpha - E_k \sim 40$ MeV and 60 MeV. Actually, the strength function (19) combines two types of information: the density of configurations and the mixing coefficients whose values are determined by the nucleon-nucleon interaction. In order to disentangle these effects, we calculate the density of configurations $\rho(E) = \sum_{k,\alpha} \delta(E - \mathcal{E}_\alpha)$ and the locally normalized strength function $\langle F_k(E)\rangle/\rho(E)$ where $\langle F_k(E)\rangle = \sum_k F_k(E)/N$. These quantities are shown in Fig. 8 [the density of configurations, upper panel (a), and the locally normalized strength function in logarithmic scale, lower panel (b)]. The configuration density has a regular shape expected for a finite Hilbert space whereas the bumps of the strength function in Fig. 7 appear magnified on the normalized strength function plot (lower panel). One also notices that the coupling of matrix elements is fully exponential (linear on logarithmic scale), if one forgets about the bumps. As the density of configuration is quasilinear in logarithmic scale at large energy, one understands the exponential convergence behavior of the strength function observed on Fig. 7. The two bumps come from the specific interaction rather than from the statistics. The matrix elements that are responsible for the bumps correspond to the same proton-neutron ME discussed

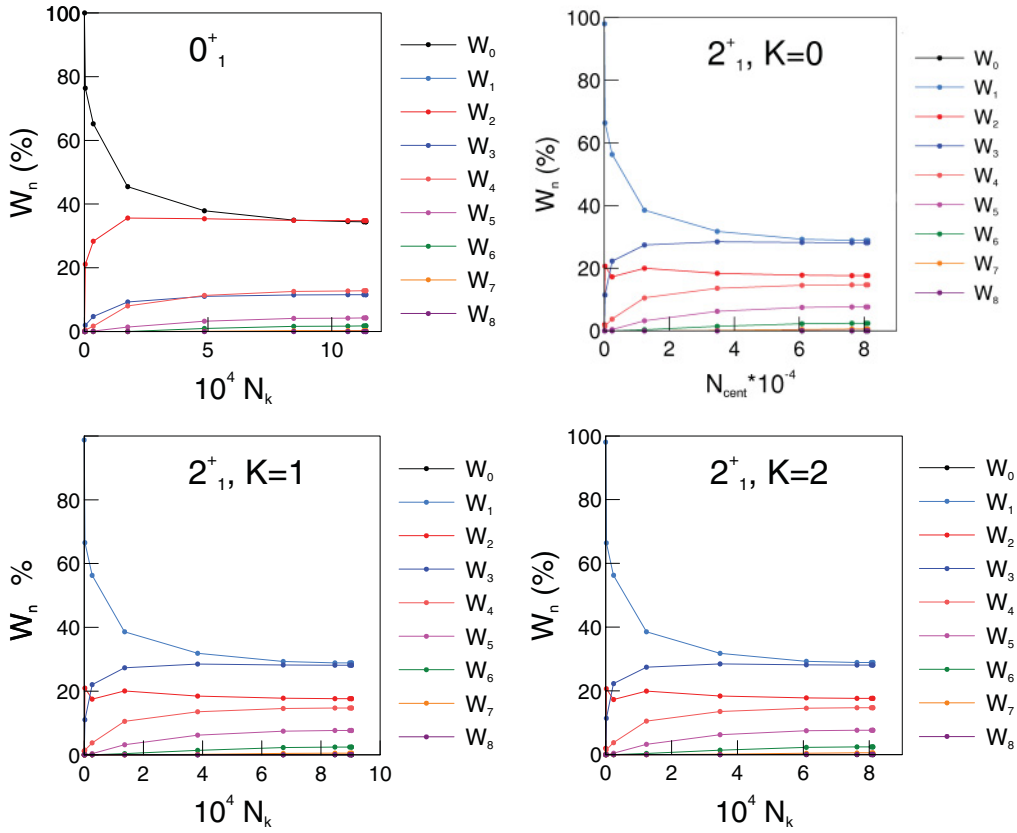

FIG. 10. (Color online) The W_i components [Eq. (13)] of 0_1^+ and 2_1^+ wave functions in ^{28}Si.

in Sec. III B for ^{30}Si, which appear to be too large at the level of the approximate resolution of the mp-mh configuration mixing method presented in this study. Reducing by hand the values of these proton-neutron ME makes the bumps disappear. Hence, the study of the chaotic behavior of highly excited Slater determinants can be considered as an additional way of highlighting not well-calibrated coupling ME. In other words, statistical properties may serve as an additional criterion in the validation process of phenomenological effective interactions. This result is consistent with and confirms our previous discussion of Sec. III B. This analysis is similar in spirit to the statistical search of interaction matrix elements responsible for the equilibrium prolate deformation [32].

The exponential convergence observed in Fig. 8 is an interesting feature that might be evaluated analytically in the particular case of the finite-range Gogny interaction. For example, taking the single-particle states as plane waves, the two-body matrix elements of the Brink-Boecker part of the Gogny force read

$$\begin{aligned}&\langle\phi_1\phi_2|e^{-(\vec{r}_1-\vec{r}_2)^2/\mu^2}|\phi_3\phi_4\rangle\\&\quad=\int\frac{d^3r_1\,d^3r_2}{(2\pi)^6}\,e^{-i\vec{k}_1\cdot\vec{r}_1}e^{-i\vec{k}_2\cdot\vec{r}_2}e^{-(\vec{r}_1-\vec{r}_2)^2/\mu^2}e^{i\vec{k}_3\cdot\vec{r}_1}e^{i\vec{k}_4\cdot\vec{r}_2}\\&\quad=\int\frac{d^3r_1\,d^3r_2}{(2\pi)^6}\,e^{-i(\vec{k}_1-\vec{k}_2)\cdot(\vec{r}_1-\vec{r}_2)}e^{-(\vec{r}_1-\vec{r}_2)^2/\mu^2}.\end{aligned}\tag{22}$$

where we have used the conservation law $\vec{k}_1+\vec{k}_2=\vec{k}_3+\vec{k}_4$.

Equation (22) reduces to the Fourier transform of a Gaussian,

$$\langle\phi_1\phi_2|e^{-(\vec{r}_1-\vec{r}_2)^2/\mu^2}|\phi_3\phi_4\rangle=\frac{\mu}{\sqrt{2}}\,e^{-\frac{m\mu^2}{2}E},\tag{23}$$

with $E=k^2/2m$ and $\vec{k}=\vec{k}_1-\vec{k}_2$. Thus, the matrix element behaves, in the case of the Gogny interaction, as a decreasing exponential with respect to excitation energy. The value of the two ranges introduced in the Gogny interaction may serve as a guide to decide an upper limit where the exponential convergence regime settles. However, this behavior exists for any physically reasonable interaction as revealed in shell model calculations [12–16].

Below we give three examples of exponential convergence behavior with increasing excitation energy of configurations, namely for the total energy, for the components of the correlated wave functions and for the occupation probabilities. Figure 9 displays the evolution of the total energies of the ground and excited states in ^{28}Si, according to the number of configurations in the correlated wave function, ordered by increasing centroid energies. The four plots correspond to the different values of the total momentum projection K. In all cases, the total energy changes rapidly when only a few Slater determinants with lowest energy are included. Then, for a larger number of configurations a smooth regime settles, a behavior independent of the value of K.

In Fig. 10, the evolution of the global components, W_n, Eq. (13), of the wave functions of the 0_1^+ and 2_1^+ states in

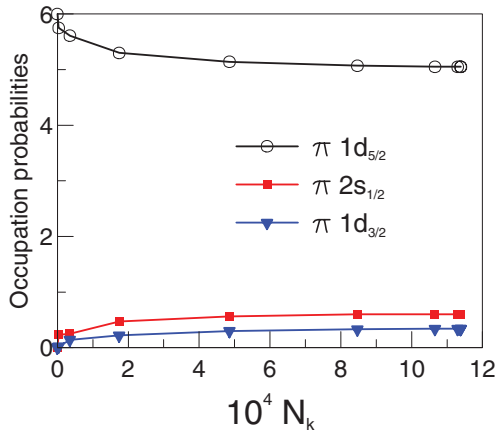

FIG. 11. (Color online) Evolution of the occupation probabilities of proton $d_{5/2}$, $s_{1/2}$, and $d_{3/2}$ orbitals as function of N_k.

^{28}Si is displayed as a function of the number N_{cent} of centroids ordered by centroid energy. For $n \geqslant 9$, the W_n are smaller than 10^{-9} and they are not shown. The evolution of the occupation probabilities for $d_{5/2}$, $s_{1/2}$, and $d_{3/2}$ orbitals according to N_{cent} is displayed on Fig. 11. As can be seen from the two figures, both the W_n and the occupation probabilities display the exponential convergence. With all exponents being close, one can loosely interpret this behavior as a signature of thermalization in a self-bound mesoscopic system.

V. CONCLUSION AND PERSPECTIVES

In this work, we have investigated the application of multiconfiguration methods for the description of low-energy nuclear spectroscopy. A few even-even silicon isotopes have been studied, using the D1S Gogny interaction. At this stage, only the configuration mixing part of the method has been put into place; the renormalization of single-particle orbitals due to correlations has not been discussed in this paper. The results for the positive parity states in low-lying spectroscopy of $^{26-32}$Si have been found in rather good agreement with experiment, taking into account the fact that the D1S Gogny interaction has not been *a priori* fitted to be employed in such a kind of approach. In particular, from the study of ^{30}Si, it has been found that, at the level of approximate resolution of the mp-mh configuration mixing method (no renormalization of orbitals) a few residual proton-neutron matrix elements of pairing type, that are not constrained in the fitting of the Gogny interaction, might disturb the reproduction of excitation energies. In relation to this, the importance and magnitude of the proton-neutron residual interaction has been discussed.

The question of the pertinent configurations that have to be introduced in the mixing has also been addressed. Statistical generic behavior of highly excited configurations has been put forward. In particular, the exponential convergence already revealed in shell model studies has been confirmed in our approach. This is an encouraging feature that may help to handle the very large number of configurations that appear in multiconfiguration methods, in particular in nuclear physics where two kinds of particles exist.

The present study proposes interesting and challenging issues at different levels. The renormalization of orbitals under the influence of correlations is an important question that will be analyzed in further studies. In atomic physics, this renormalization has been proved to play a key role in strongly correlated systems. Even though the associated orbital equation, see Eq. (8), looks simple, its exact solution is far from being trivial. At present, in the most advanced applications to atomic physics, it is solved approximately as the correlation term that depends on the two-body density matrix can be very complicated.

A second issue concerns the improvement of the Gogny interaction in order to be able to use it not only in HFB, RPA, and GCM-type methods but also in multiconfiguration approaches. Work is in progress in this direction.

The third issue deals with the generic behavior of highly excited configurations. The exponential convergence and corresponding extrapolations can be of considerable help for controlling in a safe way possible new truncation schemes introducing explicitly only pertinent configurations. To this aim, a formalism of the Feshbach type projection might be quite useful. It is worth mentioning that the analysis of statistical regularities allowed us to identify specific matrix elements of the Hamiltonian responsible for spectroscopic inadequacy (discussion on ^{30}Si).

For the specific goal of nuclear spectroscopy, the investigation of transition probabilities and negative parity states in silicon isotopes would be of great interest and may provide essential information on the residual interaction and properties of single-particle orbitals, including nuclei far from stability.

ACKNOWLEDGMENTS

N.P. would like to thank the National Superconducting Cyclotron Laboratory at Michigan State University for hospitality and B. A. Brown for providing the shell model matrix elements and results that were of great help for the analysis presented in this work. N.P. is also grateful to M. Girod and J. Libert for providing with 5DCH results and A. Zuker and M. Dufour for interesting discussions. V.Z. acknowledges the support from the NSF grants no. PHY-0758099 and PHY-1068217. Part of the calculations were carried out on CCRT supercomputers of CEA-DAM Ile de France.

APPENDIX: "CORE + VALENCE SPACE" FORMULATION

Equations (2) and (5) are quite general. As mentioned in the Introduction, the Hilbert space has to be truncated in any realistic calculation. Several truncation schemes, supported by physics arguments, can be utilized, for example a limitation on the excitation order of mp-mh configurations, a limitation in the number of single-particle states used for the configuration mixing, etc. This appendix deals with a truncation that corresponds to the description in terms of "core + valence space". In this approach, the system, that comprises N^τ nucleons of each isospin, is separated into:

(i) an even-even core where the N_c^τ lower individual states are fully occupied for each isospin;

(ii) a set of active orbitals containing $N^\tau - N_c^\tau$ particles for each isospin;
(iii) a set of unoccupied higher-energy individual states for each isospin.

Under this prescription, the proton and neutron Slater determinants, Eq. (3), are defined as

$$\left|\Phi_{\alpha_\tau}\right\rangle = \prod_{j=N_c^\tau+1}^{N^\tau} a_j^+ \prod_{i=1}^{N_c^\tau} a_i^+ |0\rangle = \prod_{j=N_c^\tau+1}^{N^\tau} a_j^+ \left|\Phi_{c_\tau}\right\rangle, \quad \text{(A1)}$$

where $|\Phi_{c_\tau}\rangle$ is the part of the wave function that describes the core.

In addition, the Hamiltonian $\hat{H}(\rho)$, Eq. (1), can be written by separating isospin contributions as

$$\hat{H}(\rho) = \sum_{\tau=\pi,\nu} \hat{H}^\tau + \hat{V}^{\pi\nu}(\rho). \quad \text{(A2)}$$

Then, from Eq. (6),

$$\hat{\mathcal{H}}(\rho) = \sum_{\tau=\pi,\nu} \left[\hat{H}^\tau + \sum_{mn\tau} \mathcal{R}^\tau_{mn} a^+_{\tau m} a_{\tau n}\right] + \hat{V}^{\pi\nu}(\rho), \quad \text{(A3)}$$

where the generalized rearrangement coefficients $\mathcal{R}^\tau_{ij}$ are given by

$$\mathcal{R}^\tau_{mn} = \int \phi^*_{\tau m}(\vec{r},\sigma)\phi_{\tau n}(\vec{r},\sigma)B(\vec{r})d^3\vec{r}, \quad \text{(A4)}$$

with $\phi_{\tau i}$ the single-particle wave functions. The difficulties in the calculation of $\mathcal{R}^\tau_{mn}$ come from the evaluation of the rearrangement field $B(\vec{r})$ from the correlated wave function (2):

$$B(\vec{r}) = \sum_{\alpha\alpha'} A^*_{\alpha'_\pi\alpha'_\nu} A_{\alpha_\pi\alpha_\nu} \sum_{ijkl} \left\langle i_{\alpha'_\pi} j_{\alpha'_\nu}\right| \frac{\partial V(\rho)}{\partial\rho(\vec{r})} \left|k_{\widetilde{\alpha_\pi}} l_{\alpha_\nu}\right\rangle \times \left\langle \Phi_{\alpha'_\pi}\right| a^+_{i_{\alpha'_\pi}} a_{k_{\alpha_\pi}} \left|\Phi_{\alpha_\pi}\right\rangle \left\langle \Phi_{\alpha'_\nu}\right| a^+_{j_{\alpha'_\nu}} a_{l_{\alpha_\nu}} \left|\Phi_{\alpha_\nu}\right\rangle. \quad \text{(A5)}$$

The expressions (A2), (A3), and (A5) are specific to the D1S Gogny interaction as only the proton-neutron terms are generated by the density-dependent part of the interaction and the density-dependence is a contact interaction. In the limit of no configuration mixing, one recovers the standard HF expression for the rearrangement term.

From Eq. (A3), one derives explicit expressions for $\mathcal{H}_{\alpha_\pi\alpha_\nu,\alpha'_\pi\alpha'_\nu}$ in terms of the "core + valence space" formulation. In the following evaluation of $\mathcal{H}_{\alpha_\pi\alpha_\nu,\alpha'_\pi\alpha'_\nu}$, only the terms carrying the core contributions are given.

1. Proton and neutron diagonal contributions

The proton and neutron diagonal contributions are obtained for $|\Phi_{\alpha_\pi}\rangle \equiv |\Phi_{\alpha'_\pi}\rangle$ and $|\Phi_{\alpha_\nu}\rangle \equiv |\Phi_{\alpha'_\nu}\rangle$ as

$$\mathcal{H}^\tau_{\alpha_\pi\alpha_\nu,\alpha_\pi\alpha_\nu} = \left\langle \phi_{\alpha_\tau}\right| \hat{H}^\tau \left|\phi_{\alpha_\tau}\right\rangle + \sum_{mn} \mathcal{R}^\tau_{mn} \left\langle \phi_{\alpha_\tau}\right| a^+_m a_n \left|\phi_{\alpha_\tau}\right\rangle \quad \text{(A6)}$$

which yields

$$\mathcal{H}^\tau_{\alpha_\pi\alpha_\nu,\alpha_\pi\alpha_\nu} = \sum_{i_{\alpha_\tau}=1}^{N^\tau} \left(\left\langle i_{\alpha_\tau}\right| K \left|i_{\alpha_\tau}\right\rangle + \mathcal{R}^\tau_{i_{\alpha_\tau} i_{\alpha_\tau}}\right) + \frac{1}{2} \sum_{i,j=1}^{N^\tau} \left\langle i_{\alpha_\tau} j_{\alpha_\tau}\right| V(\rho) \left|i_{\alpha_\tau} \widetilde{j_{\alpha_\tau}}\right\rangle. \quad \text{(A7)}$$

In Eq. (A7), i_{α_τ} stands for the occupied single-particle state in the $|\Phi_{\alpha_\tau}\rangle$ Slater determinant. The "core + valence space" separation then leads to

$$\begin{aligned}\mathcal{H}^\tau_{\alpha_\pi\alpha_\nu,\alpha_\pi\alpha_\nu} &= \sum_{i_{\alpha_\tau}=1}^{N_c^\tau} \left(\left\langle i_{\alpha_\tau}\right| K \left|i_{\alpha_\tau}\right\rangle + \mathcal{R}^\tau_{i_{\alpha_\tau} i_{\alpha_\tau}}\right) \\ &+ \sum_{i_{\alpha_\tau}=N_c^\tau+1}^{N^\tau} \left(\left\langle i_{\alpha_\tau}\right| K \left|i_{\alpha_\tau}\right\rangle + \mathcal{R}^\tau_{i_{\alpha_\tau} i_{\alpha_\tau}}\right) \\ &+ \frac{1}{2} \sum_{i_{\alpha_\tau}=1}^{N_c^\tau} \sum_{j_{\alpha_\tau}=1}^{N_c^\tau} \left\langle i_{\alpha_\tau} j_{\alpha_\tau}\right| V \left|i_{\alpha_\tau} \widetilde{j_{\alpha_\tau}}\right\rangle \\ &+ \frac{1}{2} \sum_{i_{\alpha_\tau}=N_c^\tau+1}^{N^\tau} \sum_{j_{\alpha_\tau}=N_c^\tau+1}^{N^\tau} \left\langle i_{\alpha_\tau} j_{\alpha_\tau}\right| V \left|i_{\alpha_\tau} \widetilde{j_{\alpha_\tau}}\right\rangle \\ &+ \sum_{i_{\alpha_\tau}=1}^{N_c^\tau} \sum_{j_{\alpha_\tau}=N_c^\tau+1}^{N^\tau} \left\langle i_{\alpha_\tau} j_{\alpha_\tau}\right| V \left|i_{\alpha_\tau} \widetilde{j_{\alpha_\tau}}\right\rangle. \end{aligned} \quad \text{(A8)}$$

In Eq. (A8), the first and third terms are pure core contributions. The second and forth terms are the contributions from the valence space. The mixed fifth term includes single-particle orbitals of both the core and the valence space.

2. Proton-neutron diagonal contribution

The proton-neutron diagonal contribution is obtained for $|\Phi_{\alpha_\pi}\rangle \equiv |\Phi_{\alpha'_\pi}\rangle$ and $|\Phi_{\alpha_\nu}\rangle \equiv |\Phi_{\alpha'_\nu}\rangle$, as

$$\mathcal{H}^{\pi\nu}_{\alpha_\pi\alpha_\nu,\alpha_\pi\alpha_\nu} = \left\langle \Phi_{\alpha_\pi}\Phi_{\alpha_\nu}\right| \hat{V}^{\pi\nu} \left|\Phi_{\alpha_\pi}\Phi_{\alpha_\nu}\right\rangle. \quad \text{(A9)}$$

Expansion of Eq. (A9) yields

$$\mathcal{H}^{\pi\nu}_{\alpha_\pi\alpha_\nu,\alpha_\pi\alpha_\nu} = \sum_{i=1}^{N^\pi} \sum_{j=1}^{N^\nu} \left\langle i_{\alpha_\pi} j_{\alpha_\nu}\right| V \left|i_{\alpha_\pi} \widetilde{j_{\alpha_\nu}}\right\rangle. \quad \text{(A10)}$$

Making the "core + valence space" separation leads to

$$\begin{aligned}\mathcal{H}^{\pi\nu}_{\alpha_\pi\alpha_\nu,\alpha_\pi\alpha_\nu} &= \sum_{i_{\alpha_\pi}=1}^{N_c^\pi} \sum_{j_{\alpha_\nu}=1}^{N_c^\nu} \left\langle i_{\alpha_\pi} j_{\alpha_\nu}\right| V \left|i_{\alpha_\pi} \widetilde{j_{\alpha_\nu}}\right\rangle \\ &+ \sum_{i_{\alpha_\pi}=N_c^\pi+1}^{N^\pi} \sum_{j_{\alpha_\nu}=N_c^\nu+1}^{N^\nu} \left\langle i_{\alpha_\pi} j_{\alpha_\nu}\right| V \left|i_{\alpha_\pi} \widetilde{j_{\alpha_\nu}}\right\rangle \\ &+ \sum_{i_{\alpha_\pi}=1}^{N_c^\pi} \sum_{j_{\alpha_\nu}=N_c^\nu+1}^{N^\nu} \left\langle i_{\alpha_\pi} j_{\alpha_\nu}\right| V \left|i_{\alpha_\pi} \widetilde{j_{\alpha_\nu}}\right\rangle \\ &+ \sum_{i_{\alpha_\pi}=N_c^\pi+1}^{N^\pi} \sum_{j_{\alpha_\nu}=1}^{N_c^\nu} \left\langle i_{\alpha_\pi} j_{\alpha_\nu}\right| V \left|i_{\alpha_\pi} \widetilde{j_{\alpha_\nu}}\right\rangle. \end{aligned} \quad \text{(A11)}$$

In Eq. (A11), the first term comes from the core and the second one from the valence space. The last two terms express the coupling between the core and the valence particles.

3. Proton and neutron non-diagonal one-body contributions

The proton or neutron one-body contributions arise when $|\Phi_{\alpha_\pi}\rangle$ and $|\Phi_{\alpha'_\pi}\rangle$ differ in one particle state and $|\Phi_{\alpha_\nu}\rangle \equiv |\Phi_{\alpha'_\nu}\rangle$ or when $|\Phi_{\alpha_\nu}\rangle$ and $|\Phi_{\alpha'_\nu}\rangle$ differ from one particle state and $|\Phi_{\alpha_\pi}\rangle \equiv |\Phi_{\alpha'_\pi}\rangle$, respectively. Then, the contributions to $\mathcal{H}$ are

$$\mathcal{H}^1_{\alpha_\pi\alpha_\nu,\alpha'_\pi\alpha_\nu} = \sum_{i_{\alpha_\pi}=1}^{N_c^\pi} \langle i_{\alpha_\pi} j_{\alpha'_\pi} | V | i\widetilde{\alpha_\pi l_{\alpha'_\pi}} \rangle + \sum_{i_{\alpha_\pi}=N_c^\pi+1}^{N^\pi} \langle i_{\alpha_\pi} j_{\alpha'_\pi} | V | i\widetilde{\alpha_\pi l_{\alpha'_\pi}} \rangle \quad \text{(A12)}$$

and

$$\mathcal{H}^1_{\alpha_\pi\alpha_\nu,\alpha_\pi\alpha'_\nu} = \sum_{i_{\alpha_\nu}=1}^{N_c^\nu} \langle i_{\alpha_\nu} j_{\alpha'_\nu} | V(\rho) | i\widetilde{\alpha_\nu l_{\alpha'_\nu}} \rangle + \sum_{i_{\alpha_\nu}=N_c^\nu+1}^{N^\nu} \langle i_{\alpha_\nu} j_{\alpha'_\nu} | V(\rho) | i\widetilde{\alpha_\nu l_{\alpha'_\nu}} \rangle. \quad \text{(A13)}$$

In Eqs. (A12) and (A13), the indices j and l refer to the single-particle state different between the configurations α and α'. The first term in Eqs. (A12) and (A13) corresponds to the core contribution and the second one to the contribution of the valence space.

4. Proton-neutron nondiagonal one-body contribution

As for the proton and neutron one-body contributions, the proton-neutron one-body contribution arises when $|\Phi_{\alpha_\pi}\rangle$ and $|\Phi_{\alpha'_\pi}\rangle$ differ by one particle state and $|\Phi_{\alpha_\nu}\rangle \equiv |\Phi_{\alpha'_\nu}\rangle$ or when $|\Phi_{\alpha_\nu}\rangle$ and $|\Phi_{\alpha'_\nu}\rangle$ differ by one particle state and $|\Phi_{\alpha_\pi}\rangle \equiv |\Phi_{\alpha'_\pi}\rangle$. Similarly to Eqs. (A12) and (A13), the proton-neutron nondiagonal one-body contribution is then given by

$$\mathcal{H}^{1\tau'}_{\alpha_\tau\alpha_{\tau'},\alpha_\tau\alpha'_{\tau'}} = \sum_{i_{\alpha_\tau}=1}^{N_c^\tau} \langle i_{\alpha_\tau} j_{\alpha_{\tau'}} | V^{\pi\nu}(\rho) | i\widetilde{\alpha_\tau l_{\alpha'_{\tau'}}} \rangle + \sum_{i_{\alpha_\tau}=N_c^\tau+1}^{N^\tau} \langle i_{\alpha_\tau} j_{\alpha_{\tau'}} | V^{\pi\nu}(\rho) | i\widetilde{\alpha_\tau l_{\alpha'_{\tau'}}} \rangle. \quad \text{(A14)}$$

In Eq. (A14), the indices j and l refer to the single-particle states that differ between the configurations α and α'. Still, the first term describes the core contribution and the second one the contribution of the valence space.

[1] P. Ring and P. Schuck, *The Nuclear Many-Body Problem* (Springer-Verlag, New York, 1980).
[2] M. Anguiano, J. L. Egido, and L. M. Robledo, Nucl. Phys. A **696**, 467 (2001).
[3] M. Anguiano, J. L. Egido, and L. M. Robledo, Phys. Lett. B **545**, 62 (2002).
[4] M. Bender, G. F. Bertsch, and P.-H. Heenen, Phys. Rev. C **73**, 034322 (2006).
[5] M. Bender and P.-H. Heenen, Phys. Rev. C **78**, 024309 (2008).
[6] T. R. Rodriguez, J. L. Egido, L. M. Robledo, and R. Rodriguez-Guzman, Phys. Rev. C **71**, 044313 (2005).
[7] R. Rodriguez-Guzman, L. Egido, and L. M. Robledo, Nucl. Phys. A **709**, 201 (2002).
[8] T. R. Rodriguez and J. L. Egido, Phys. Rev. C **81**, 064323 (2010).
[9] J.-P. Delaroche, M. Girod, J. Libert, H. Goutte, S. Hilaire, S. Péru, N. Pillet, and G. F. Bertsch, Phys. Rev. C **81**, 014303 (2010).
[10] N. Pillet, J.-F. Berger, and E. Caurier, Phys. Rev. C **78**, 024305 (2008).
[11] N. Pillet, P. Quentin, and J. Libert, Nucl. Phys. A **697**, 141 (2002).
[12] M. Horoi, B. A. Brown, and V. Zelevinsky, Phys. Rev. C **50**, R2274 (1994).
[13] V. Zelevinsky, B. A. Brown, N. Frazier, and M. Horoi, Phys. Rep. **276**, 85 (1996).
[14] M. Horoi, A. Volya, and V. Zelevinsky, Phys. Rev. Lett. **82**, 2064 (1999).
[15] M. Horoi, B. A. Brown, and V. Zelevinsky, Phys. Rev. C **67**, 034303 (2003).
[16] M. Horoi, J. Kaiser, and V. Zelevinsky, Phys. Rev. C **67**, 054309 (2003).
[17] S. Pittel and B. Thakur, Rev. Mex. Fis. S **55**(2), 0108 (2009).
[18] S. Pittel and N. Sandulescu, Phys. Rev. C **73**, 014301 (2006).
[19] J. Rotureau, N. Michel, W. Nazarewicz, M. Ploszajczak, and J. Dukelsky, Phys. Rev. Lett. **97**, 110603 (2006).
[20] T. Papenbrock and D. J. Dean, J. Phys. G **31**, S1377 (2005).
[21] J. Dukelsky, S. Pittel, S. S. Dimitrova, and M. V. Stoitsov, Phys. Rev. C **65**, 054319 (2002).
[22] T. Otsuka, M. Honma, T. Mizusaki, N. Shimizu, and Y. Utsuno, Prog. Part. Nucl. Phys. **47**, 319 (2001).
[23] J. Dechargé and D. Gogny, Phys. Rev. C **21**, 1568 (1980); J.-F. Berger, M. Girod, and D. Gogny, Comput. Phys. Commun. **63**, 365 (1991).
[24] J. Libert, M. Girod, and J.-P. Delaroche, Phys. Rev. C **60**, 054301 (1999).
[25] A. Obertelli, S. Péru, J.-P. Delaroche, A. Gillibert, M. Girod, and H. Goutte, Phys. Rev. C **71**, 024304 (2005).
[26] T. Otsuka, R. Fujimoto, Y. Utsuno, B. A. Brown, M. Honma, and T. Mizusaki, Phys. Rev. Lett. **87**, 082502 (2001).
[27] T. Otsuka, Y. Utsuno, R. Fujimoto, B. A. Brown, M. Honma, and T. Mizusaki, Eur. Phys. J. A **13**, 69 (2002).
[28] N. A. Smirnova, A. De Maesschalck, A. Van Dyck, and K. Heyde, Phys. Rev. C **69**, 044306 (2004).
[29] M. Anguiano (private communication).
[30] B. H. Wildenthal, Prog. Part. Nucl. Phys. **11**, 5 (1984).
[31] R. A. Sen'kov, M. Horoi, and V. Zelevinsky, Phys. Lett. B **702**, 413 (2011).
[32] M. Horoi and V. Zelevinsky, Phys. Rev. C **81**, 034306 (2010).